Soft Materials that Intercept, Respond to, and Sequester Bacterial Siderophores

Benjamin J. Ortiz,[1] James Jennings,[2,†] William S. Gross,[3] Thiago M. A. Santos,[3] Ti-Yu Lin,[3] Douglas B. Weibel,[2,3,4,*] and David M. Lynn[1,2,*]

[1]*Department of Chemical and Biological Engineering, 1415 Engineering Dr., University of Wisconsin–Madison, Madison, WI 53706, USA;* [2]*Department of Chemistry, 1101 University Ave., University of Wisconsin–Madison, Madison, WI 53706, USA;* [3]*Department of Biochemistry, 433 Babcock Dr., University of Wisconsin–Madison, Madison, WI 53706, USA;* [4]*Department of Biomedical Engineering, 1550 Engineering. Dr., University of Wisconsin–Madison, Madison, WI 53706, USA; Current Address:* Institute of Molecular Biosciences, Humboldtstraße 50, University of Graz, Graz 8010, Austria; [*]*Email: (D.B.W.)* douglas.b.weibel@gmail.com; *(D.M.L.) dlynn@engr.wisc.edu*

ABSTRACT: We report the design and characterization of Fe-containing soft materials that respond to, interface with, and/or sequester Fe-chelating 'siderophores' that bacteria use to scavenge for iron and regulate iron homeostasis. We demonstrate that metal-organic network coatings fabricated by crosslinking tannic acid with iron(III) are stable in bacterial growth media, but erode upon exposure to biologically relevant concentrations of enterobactin and deferoxamine B, two siderophores produced by Gram-negative and Gram-positive bacteria, respectively. Our results are consistent with changes in network stability triggered by the extraction of iron(III) and reveal rates of siderophore-induced disassembly to depend upon both siderophore concentration and affinity for iron(III). These coatings also disassemble when incubated in the presence of cultures of wild-type *Escherichia coli*. Assays using genetically modified strains of *E. coli* reveal the erosion of these materials by live cultures to be promoted by secretion of enterobactin and not from other factors resulting from bacterial growth and metabolism. This stimuli-responsive behavior can also be exploited to design coatings that release the Fe-chelating antibiotic ciprofloxacin into bacterial cultures. Finally, we report the discovery of Fe-containing polymer hydrogels that avidly sequester and scavenge enterobactin from surrounding media. The materials reported here are (i) capable of interfacing or interfering with mechanisms that bacteria use to maintain iron homeostasis, either by yielding iron to or by sequestering iron-scavenging agents from bacteria, and can (ii) respond dynamically to or report on the presence of populations of iron-scavenging bacteria. Our results thus provide new tools that could prove useful for microbiological research and enable new stimuli-responsive strategies for interfacing with or controlling the behaviors of communities of iron-scavenging bacteria.

Introduction

In this paper, we report the design of iron-containing soft materials, including metal-organic network coatings and polymer-based hydrogels, that can interact with, respond to, and sequester chemical 'siderophores' that many bacteria use to scavenge for iron and carry out important biological processes. The materials and approaches reported here provide tools that could prove useful for microbiological research and provide guidance for the design of new stimuli-responsive materials that can interface with or directly influence the behaviors of communities of iron-scavenging bacteria.

Bacteria have evolved sophisticated mechanisms to assess their environment and carry out processes vital for survival and adaptation to hostile or changing environments. One such mechanism is the regulation of iron homeostasis, which bacteria use to manipulate concentrations of intracellular iron.[1] In iron-rich environments, this process helps bacteria maintain amounts of iron needed for metabolism, biosynthesis, and other processes without exceeding levels that are toxic.[1] In iron-poor environments, bacteria use several mechanisms to forage for iron, including lowering environmental pH to increase ferric iron (Fe^{III}) solubility.[1,2] When iron is scarce, many species of bacteria also upregulate the synthesis and secretion of iron-chelating 'siderophores' that can coordinate strongly to extracellular Fe^{III} and re-enter cells *via* active transport.[1-3] This latter process is regulated predominantly by the ferric uptake regulator (FUR) protein,[1-5] but an emerging body of work suggests that siderophore production, and thus iron homeostasis, may also be regulated in some species by control of quorum sensing.[2,6-10] Regardless of the governing mechanism, siderophores play critical roles in enabling bacterial virulence and constitute shared tools for the gathering of resources within bacterial communities by providing an essential nutrient needed for bacterial growth and biosynthesis.[1,11]

The most commonly exploited triggers used to design materials that respond to the presence of bacteria include changes in environmental pH, the expression of enzymes (*e.g.,* lipases, phosphatase, and hyaluronidase), and the production of pore-forming toxins.[12-19] Despite a growing body of knowledge highlighting links between iron homoeostasis and bacterial virulence,[11,20] the design of materials that can interface with bacteria by exploiting the functions of siderophores has not been widely explored. Siderophores are produced by many different Gram-negative and Gram-positive bacteria and are avid binders of environmental iron; some are, indeed, among the strongest chelators of Fe^{III} known (*e.g.,* $k_a = 10^{49}$ for enterobactin, a siderophore produced by *Escherichia coli*; Figure 1, left).[21] We reasoned that siderophores could be used to extract iron from iron-containing materials and that, if designed appropriately (*e.g.,* if iron were used as a key structural element of the material) it should be possible to create materials that undergo changes in properties or behavior upon exposure to iron-scavenging

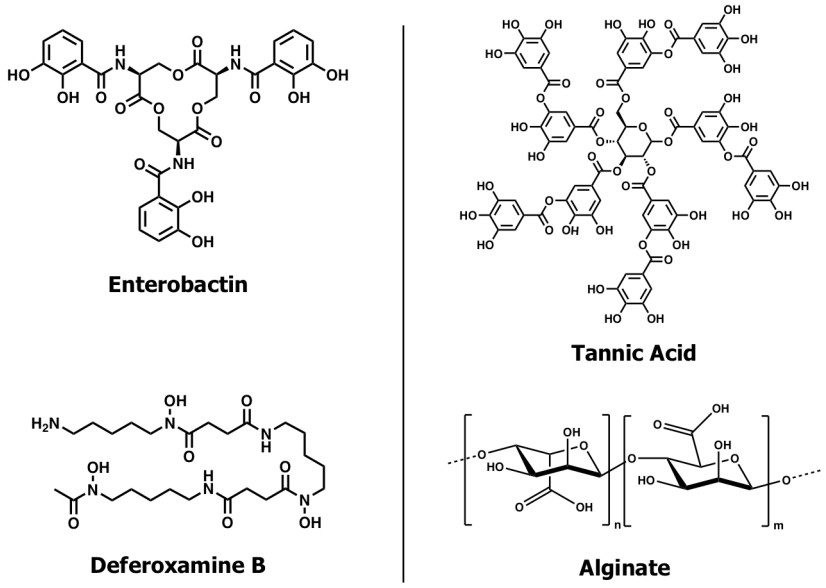

Figure 1. Structures of enterobactin and deferoxamine B, the two bacterial siderophores used in this study **(**left). Structures of tannic acid and alginate, small-molecule and polymeric iron-binding organic building blocks used in this study (right).

bacteria in ways that could be useful in fundamental and applied contexts (Figure 2A). More broadly, the ability to control the exchange of iron between bacteria and soft materials could also provide new tools useful for interfacing with and influencing the behaviors of bacterial colonies by controlling, disrupting, or hijacking elements of iron homeostasis pathways that are important for growth and virulence (Figure 2B).[11]

The work reported here builds from the results of past studies demonstrating that ferric iron can be used to promote the coordination-driven assembly of polyphenols into thin films and

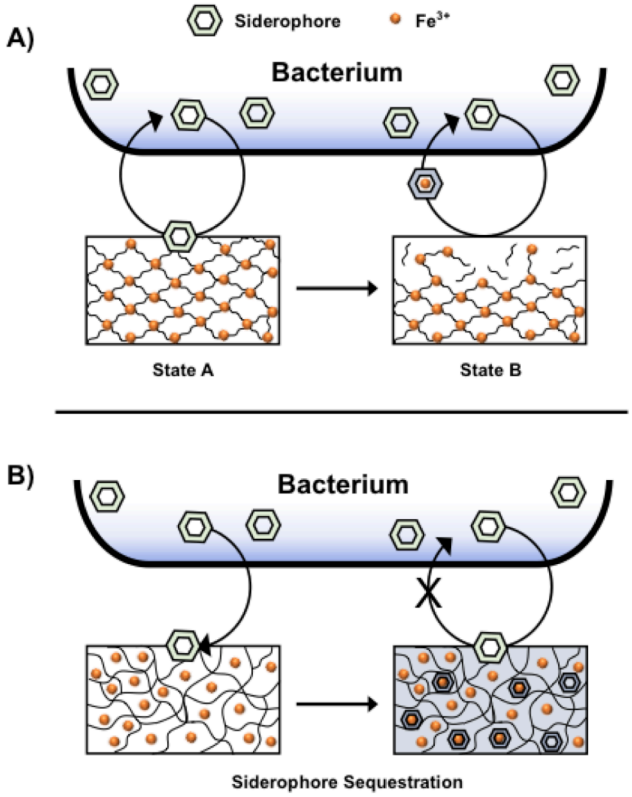

Figure 2. (A) Schematic illustration of interactions between an iron-scavenging bacterium in which siderophores (open hexagons) are secreted and interact with a material containing iron (orange spheres) as a structural element. Extraction of the iron by siderophores results in a physical change in the material from State A to State B, and siderophores shuttle extracted iron to the bacterium. (B) Schematic illustration of interactions between an iron-scavenging bacterium in which siderophores are secreted and interact with a material containing iron in a manner that results in the retention of the siderophore on or within the material, resulting in sequestration of the siderophores.

coatings.[22,23] These metal-organic networks can be deposited onto a diverse array of substrates and are of broad technological interest due to their mechanical and thermal stability,[24-26] selective permeability,[27-29] and responsiveness to changes in pH[30-32] that arise from their highly crosslinked structures and the reversible nature of the metal coordination chemistry that drives assembly.[23] Here, we demonstrate that thin metal-organic coatings fabricated from the crosslinking of the natural polyphenol tannic acid (TA; Figure 1, right) and ferric ions (referred to from hereon as TA-Fe^{III} films) that are physically stable in many aqueous environments erode slowly upon exposure to biologically relevant concentrations of two model bacterial siderophores. Our results demonstrate that siderophore-induced disassembly occurs with kinetics controlled by siderophore concentration and the affinity of the siderophores for Fe^{III}. These materials also disassemble gradually when incubated in the presence of cultures of wild-type *E. coli*. The results of additional bacterial assays using genetically modified knock-out strains of *E. coli* reveal the erosion of these materials in live cultures to be promoted predominantly by secretion of enterobactin as the bacteria forage for iron and not by other factors, such as changes in environmental pH. We further demonstrate that this stimuli-responsive behavior can be exploited to design TA-Fe^{III} films containing antibiotics that are released into bacterial cultures upon contact with siderophores. Finally, we report the unexpected discovery of Fe-containing polymer hydrogels of the natural polymer alginate that do not disassemble upon exposure to enterobactin but, instead, avidly sequester enterobactin and scavenge it from surrounding media. When combined, these results provide guidance for the design of new metal-containing materials that can respond to the presence of iron-scavenging bacteria, interface with and influence processes that govern bacterial iron homeostasis, and attenuate the behaviors of communities of bacteria.

Materials and Methods

Materials. Tannic acid (TA, ACS reagent grade), enterobactin (derived from *Escherichia coli*, ≥98%), diethyl ether (ACS reagent grade, 99%), acetonitrile (HPLC grade, 99.9%), sodium hydroxide (NaOH; ACS reagent grade, 97%), hydrochloric acid (HCl, ACS reagent, 37%), sodium phosphate dibasic (Na_2HPO_4; ACS reagent grade, 99%), Gallium (III) nitrate (99.9%), and dimethyl sulfoxide (DMSO; BioReagent grade, 99.9%) were all purchased from Sigma Aldrich (Milwaukee, WI). Citric acid (99%), iron (III) sulfate pentahydrate (97%), and sodium molybdate (VI) dihydrate (99%) were purchased from Acros Organic (New Jersey, US). Sodium nitrite (lab grade, 99%) was obtained from Ward's Science+ (Rochester, NY). Deferoxamine mesylate (DFO, 97%) was purchased from Santa Cruz Biotechnology Inc. (Dallas, TX). Ciprofloxacin HCl (molecular biology grade) was purchased from GoldBio (St. Louis, MO). Sodium alginate was obtained from Spectrum Chemical (New Brunswick, NJ). Phosphate-buffered saline (PBS, pH = 7.4, ionic strength = 154 mM) was prepared by diluting commercially available liquid concentrate (OmniPur® 10X PBS) purchased from EMD Millipore (Burlington, MA). BacTiter-Glo™ microbial cell viability assay was purchased from Promega (Madison, WI). All chemicals were used as received unless otherwise noted.

General Considerations. Deionization of distilled water was performed using a Milli-Q system (Millipore, Bedford, MA) to give water with a resistivity of 18.2 MΩ cm. Glass slides were purchased from VWR (Batavia, IL). Prior to coating with iron-crosslinked tannic acid (TA-Fe^{III}) films, glass slides were rinsed with acetone, methanol, ethanol, and water and then dried under a stream of filtered air before subjecting the substrates to plasma oxidation for 10 minutes (plasma

power 250 mW and oxygen flow rate of 50 cm^3/min). Sonication was performed using a Branson 2510 water bath sonicator at ambient temperature. Citric acid-Na_2HPO_4 buffer (pH = 2.8) was prepared by mixing 408.7 mL of 0.1M citric acid with 50 mL of 0.2M Na_2HPO_4. Absorbance readings of coatings and solutions of culture supernatants analyzed by Arnow's test were made using a Tecan Infinite M200 Pro microplate reader (Tecan, Grödig, Austria). Absorbance values were measured in five different locations set by the plate reader software, i-control 1.12, in the circle-filled configuration with a distance from the plate wall of 5000 μm for 12-well plates and 750 μm for 24-well plates. UV/vis measurements were made using an Eppendorf BioSpectrometer basic spectrophotometer (Hauppauge, NY). The optical thicknesses of TA-Fe^{III} films fabricated on silicon wafers were characterized using a Gaertner LSE ellipsometer (632.8 nm, incident angle = 70°). Data were processed using the Gaertner Ellipsometer Measurement program. To determine the relative thickness of TA-Fe^{III} films, an average refractive index of 1.56 was assumed. The silicon substrates were determined to have a refractive index of 3.85 and an extinction coefficient of -0.1342. Thicknesses for each deposition cycle were determined in at least five standardized locations on each substrate, and are reported as the average of measurements made on three independent coatings.

Bacterial Strains and Growth Conditions. Unless stated otherwise, *E. coli* strains were routinely grown aerobically in M9 minimal medium (1 × M9 salts [8.55 mM NaCl, 22 mM KH_2PO_4, 47.7 mM $Na_2HPO_4 \cdot 7H_2O$, 18.7 mM NH_4Cl] supplemented with 2 mM $MgSO_4$, 0.4% [w/v] glucose, 0.1 mM $CaCl_2$, and 2 mM all essential amino acids) (pH 7.0) or in lysogeny broth (LB) (1% [w/v] tryptone, 0.5% [w/v] yeast extract, and 1% [w/v] NaCl) at 37 °C. Kanamycin (30

μg/mL) was added to the medium or agar as needed. Bacterial strains and plasmids used in this study are listed in SI Table 1.

Preparation of TA-Fe^{III} and TA:CP-Fe^{III} Coatings. Glass slides were coated with $(TA\text{-}Fe^{III})_n$ following a procedure published by Ejima *et al.* with the following modifications.[22] Glass slides were cut to desired dimensions (1.3 cm x 7.5 cm with horizontal scoring every 1.5 cm to facilitate subsequent separation into smaller pieces after coating) and cleaned as described in the General Considerations section. Individual substrates were then placed in a 15 mL centrifuge tube and 0.02 M $Fe_2(SO_4)_3$ (704 μL) was added and diluted up to ~13 mL with milliQ water. An aqueous solution of tannic acid (1.5 mL, 4 mg/mL) was then added, after which the solution turned from a light orange to a deep blue color. The tube was immediately vortexed for 10 s, followed by the addition of 1 M NaOH (130 μL). After addition of the base, the tube was continuously vortexed for one minute. The supernatant was then decanted, and the glass slides were rinsed under a stream of milliQ water before repeating this process for the desired number of deposition cycles (n). To fabricate iron-crosslinked tannic acid coatings loaded with ciprofloxacin $(TA_x\text{:}CP_y\text{-}Fe)_n$, the same method described above was followed with the exception that mixtures of tannic acid and ciprofloxacin HCl with molar ratios of 1:1 or 1:3 (TA:CP) (*i.e.,* 2.35 mM : 2.35 mM, and 2.35 mM : 7.05 mM, respectively) were used instead of pure tannic acid.

Characterization of TA-Fe^{III} Film Erosion Induced by Enterobactin and DFO. TA-Fe^{III} coated glass slides were prepared as described above, placed in separate 50 mL centrifuge tubes, and solutions (25 mL) of enterobactin dissolved in 10% (v/v) acetonitrile in water were added.

The tubes were incubated at 37 °C, and film erosion was monitored at pre-determined time intervals by removing the slides, rinsing with milliQ water, and air drying before analyzing the absorbance at 315 nm in 10 different positions on each slide (Beckmann Coulter DU520). Control experiments in the absence of siderophore were run in parallel by adding a coated slide to 25 mL of solvent consisting of 10 % (v/v) acetonitrile in water.

Quantification of Enterobactin Concentration Bacterial Culture Supernatants. Standard solutions of enterobactin were prepared in M9 media by preparing 100 times more concentrated serially diluted stocks in DMSO and a subsequent dilution in M9 to achieve the final desired concentration containing 1% DMSO (to aid with enterobactin solubility). These solutions were then used to perform Arnow's assay, following previously described methods,[33,34] to correlate enterobactin concentrations with the absorbance signal (λ_{max} = 505 nm) that results from the nitrosation of the catechol rings.[34] Briefly, 500 μL of enterobactin solution were added to a glass test tube and mixed with 500 μL of 0.5 M HCl. This was followed by the addition of 500 μL of a mixture of sodium nitrite (0.1 g/mL) and sodium molybdate (0.1 g/mL), and subsequent addition of 500 μL of 1M NaOH. Samples were mixed by vortexing between each addition, and the absorbance of this final mixture was recorded 5 min after the addition of NaOH. This same process was performed on *E. coli* culture supernatants that were obtained by centrifuging cultures for 5 min at 2000 x g, collecting the supernatant, and then filtering it using a 0.22 μm PES syringe filter.

Characterization of the Release of Ciprofloxacin from TA:CP-Fe^{III} coatings. Standard calibration curves correlating ciprofloxacin fluorescence with concentration were obtained using

milliQ water or citric acid-Na_2HPO_4 buffer and a 24-well plate containing 1 mL of serially diluted solutions; fluorescence was measured (emission 454 nm, excitation 280 nm) using a Tecan well plate reader with gain set to 89. Glass slides coated with 10 deposition cycles of $(TA_1:CP_1\text{-}Fe)_{10}$ and $(TA_1:CP_3\text{-}Fe)_{10}$ were cleaned immediately after fabrication by rinsing with water followed by ethanol. The coated glass slides were then immersed in a 12-well plate containing 2 mL of milliQ water and incubated for pre-determined times, at which 1 mL aliquots were removed for fluorescence intensity readings. The release of ciprofloxacin in water was measured in this manner over a period of 48 hours, after which the coatings were immersed in 2 mL of citric acid-Na_2HPO_4 buffer (pH = 2.8) for one hour to promote complete coating disassembly to measure the amount of ciprofloxacin remaining in the structure. Citric acid was used here because of its Fe-chelating properties and was buffered at pH 2.8 to promote complete erosion within one hour. We also used citric acid for these studies because when enterobactin was used to induce erosion we observed the subsequent release and quenching of ciprofloxacin fluorescence, preventing accurate measurements of the amount of ciprofloxacin released from the coatings. After one hour of incubation the coatings were removed, and the fluorescence of release solution was measured.

Characterization of Antimicrobial Activity of TA:CP-Fe^{III} Coatings. Coatings of $(TA_1:CP_1\text{-}Fe)_{10}$ or $(TA\text{-}Fe)_{10}$ (negative control) were cleaned by rinsing with water, sterilized by rinsing with ethanol, dried by evaporation, and placed on a sterile 12-well plate. To each well containing the coatings, 1 mL of M9 media with 1% DMSO or 10 μM enterobactin in M9 with 1% DMSO was added. Then, wells were inoculated with *E. coli* Δ*entC* (OD_{600} = 1.00) and allowed to grow at 37 °C with orbital shaking at 200 rpm for 24 hours. After this, the viability of cells was

determined following the BacTiter-Glo manufacturer's provided protocol. Luminescence of cells after 5 minutes of incubation at 37 °C with orbital shaking was measured using Tecan well plate reader.

Preparation of Iron-Crosslinked Alginate Beads. Iron-crosslinked alginate beads were prepared using an extrusion dripping method. First, a 1% (w/v) alginate solution was prepared by dissolving dry alginate in milliQ water, facilitated by stirring overnight at ambient temperature. To prepare the Fe-alginate beads, 3 mL of the 1 % (w/v) alginate solution was collected using a 5 mL syringe, and the solution was dispensed dropwise through a 20 gauge needle into a 50 mL stirred solution of 25 mg/mL $Fe_2(SO_4)_3 \cdot 5H_2O$. The iron(III) sulfate solution was prepared by dissolving 1.25 g of $Fe_2(SO_4)_3 \cdot 5H_2O$ in 50 mL of phosphate-reduced M9 or in milliQ water. Alginate beads crosslinked with Ga^{III} were prepared following the same procedure using gallium(III) nitrate dissolved in ultrapure water (25 mg/mL). The M9 was prepared as described above with the exception that the recipe was adjusted for phosphate ions by decreasing KH_2PO_4 to 4.4 mM and $Na_2HPO_4 \cdot 7H_2O$ to 9.5 mM. The beads were allowed to cross-link for one hour, the $Fe_2(SO_4)_3 \cdot 5H_2O$ was decanted, and the beads were washed with milliQ water five times. The beads were then incubated in milliQ water for 24 hours, washed once more, and then stored in milliQ water and used within three days of preparation. This process yielded over 100 Fe-containing beads with diameters of 2.7 ± 0.4 mm.

Sequestration of Enterobactin Using Metal-Crosslinked Beads. Fe-alginate or Ga-alginate beads fabricated as described above were incubated in 1 mL of M9 buffer or water and in solutions of enterobactin at a concentration of 100 μM prepared in either water or M9 buffer.

The beads were incubated with moderate shaking at 37 °C and the supernatant was removed at pre-determined time points to record its UV/vis absorbance from 250 nm to 800 nm. Enterobactin solutions were prepared from a concentrated stock dissolved in DMSO at 10 mM and further diluted to achieve a concentration of 100 μM containing 1% (v/v) of DMSO in either water or M9. For experiments in which Fe-alginate beads were incubated directly with bacteria, beads were prepared as described above with the exception that sterile milliQ water was used to prepare alginate solutions and aseptic conditions were maintained during the preparation and subsequent handling of beads. For these experiments, three beads were transferred to the wells of a 24-well plate containing 1 mL of M9 media inoculated with *E. coli* Δ*entC* (OD_{600} = 1.00), Δ*fur* (OD_{600} = 1.00), or M9 (control) and maintained at 37 °C with orbital shaking at 200 rpm for 24 hours. Images of the beads and the wells were recorded using a digital camera.

Characterization of the Reversibility of Enterobactin Sequestration on Fe-Alginate Beads. A total of five alginate beads crosslinked with Fe^{III}, prepared as described above in water, were incubated in 1 mL of a 100 μM enterobactin solution in water for 72 hours. After this pre-incubation period, Fe-alginate beads were removed from the enterobactin solution and transferred to fresh water for an additional 24 hours, at which UV/vis absorption spectra of the supernatant were recorded from 250 nm to 800 nm periodically over 24 hours.

Results and Discussion

Siderophores Trigger the Disassembly and Erosion of TA-Fe^{III} Films in Aqueous Buffer

We performed a series of initial experiments to assess the impacts of bacterial siderophores on the behaviors of thin film coatings fabricated by the metal coordination-induced crosslinking and precipitation of TA and Fe^{III} (see schematic illustration in Figure 3A). Although a broad range of natural and synthetic small-molecule and macromolecular polyphenols have been used to design these types of metal-organic networks,[22,30,35-37] we selected TA for use in these proof-of-concept studies for several reasons: (i) coatings fabricated from TA and Fe^{III} adhere strongly to a broad range of substrates and materials, (ii) these materials can be designed to be physically stable in a variety of aqueous and physiologically relevant environments, but can be disrupted in the presence of synthetic iron-chelating agents such as EDTA,[22] (iii) TA is a natural building block that leads to Fe-crosslinked coatings that are reported to be generally biocompatible,[35,36,38] and (iv) materials derived from TA and Fe^{III} exhibit properties and behaviors that are attractive in biotechnological, pharmaceutical, and food science contexts where materials that respond to contact with iron-scavenging bacteria could be useful.[39-43]

As model siderophores, we selected enterobactin, a ubiquitous catechol-type siderophore found in Gram-negative bacterial species including *E. coli* and *Salmonella typhimurium*, and the hydroxamate-based siderophore deferoxamine B (DFO), which is produced by the Gram-positive species *Streptomyces pilosus* (Figure 1).[20,44] As noted above, enterobactin is one of the strongest known naturally occurring iron-chelators ($k_a = 10^{49}$).[21] DFO is also a strong chelator of iron, but it has an affinity constant that is 19 orders of magnitude lower than that of enterobactin ($k_a = 10^{30}$) for 1:1 complexes.[45] For all experiments described below, TA-Fe^{III} films were fabricated on the surfaces of glass slides using a TA:Fe^{III} ratio of 1 to 20 (conditions determined to lead to

coatings that were substantially stable in bacterial growth buffer; *vide infra*). We estimate the thicknesses of these films after the deposition of five cycles of TA and Fe^{III} to be ~15 nm based on measurements made using ellipsometry on otherwise identical films fabricated on reflective silicon substrates (see Figure S1 of the Supporting Information).

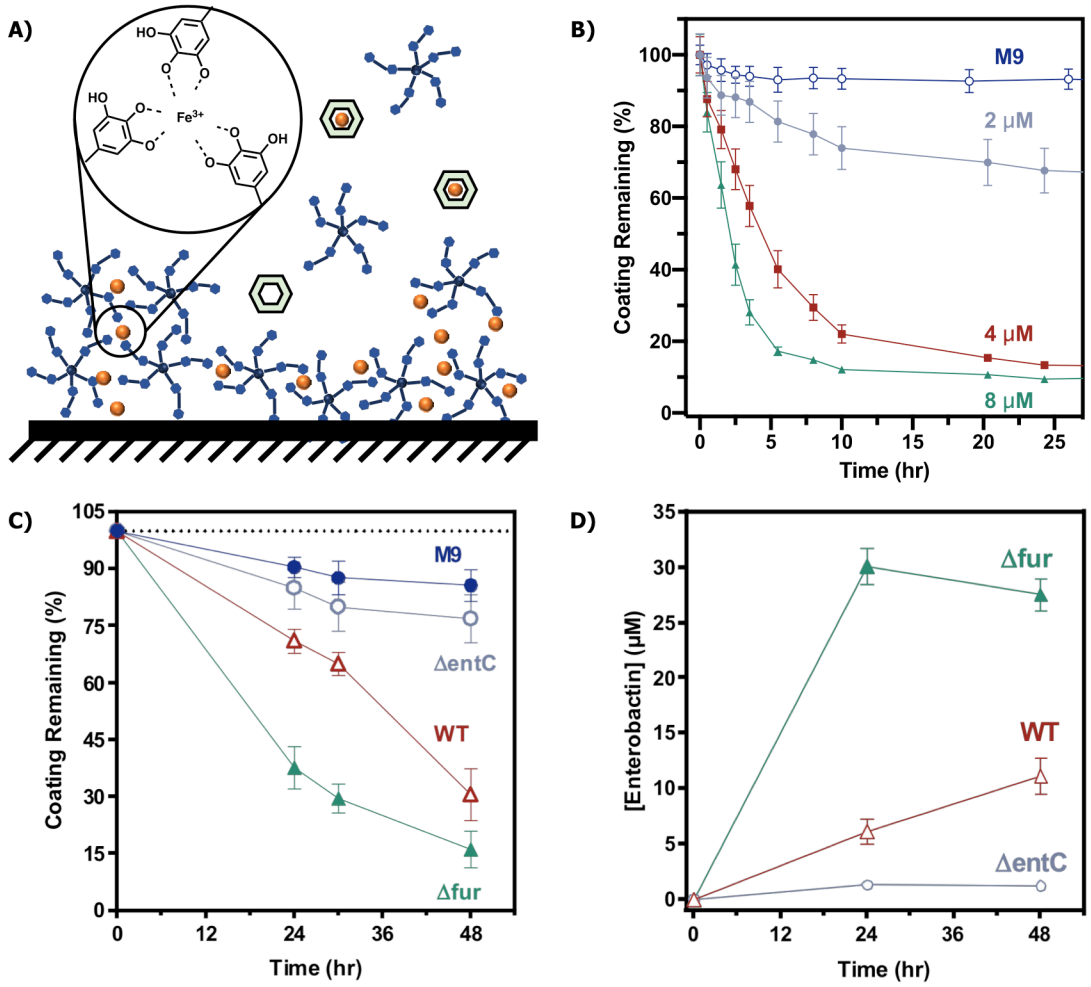

Figure 3. (A) Schematic representation of siderophore-induced erosion of iron crosslinked tannic acid coatings (TA-Fe^{III}). (B) UV/vis analysis of TA-Fe^{III} coated glass slides demonstrated that erosion takes place in the presence of enterobactin aqueous solutions containing 10% (v/v) acetonitrile at various biologically-relevant concentrations: 2 µM (filled circles), 4 µM (filled squares), and 8 µM (filled triangles); results for M9 medium are shown as open circles. (C) UV/vis analysis of TA-Fe^{III} coated glass slides showing erosion as a percentage of the coating remaining when incubated with *E. coli* strains, WT (open triangles), Δ*fur* (filled triangles), Δ*entC* (open circles), and M9 control (filled circles). (D) Enterobactin concentrations produced by different *E. coli* strains, WT (open triangles), Δ*fur* (filled triangles), and Δ*entC* (open circles) after 24 and 48 hours of growth quantified by using the liquid Arnow's test on culture supernatants. All data points in each plot represents the mean ± SEM (n = 3).

Substrates coated with TA-Fe^{III} films were incubated in solutions of enterobactin prepared in aqueous M9 buffer (containing 10% (v/v) CH_3CN to aid solubility) at concentrations of 2 to 8 μM relevant to those found in cultures of *E. coli*[46] (Figure 3B; *vide infra*), and we characterized the stability of the films over time by measuring changes in UV/vis absorption [these materials exhibit absorbance at 315 nm that is characteristic of the phenolate form of TA[47] and correlates with the thickness of TA-Fe^{III} coatings as previously described[22] (Figure S2)]. Inspection of Figure 3B reveals these films are physically stable in M9 medium for at least 24 hours, but that the presence of enterobactin leads to large decreases in the absorbance of TA that we interpret to result from the gradual erosion and loss of TA from these materials. The decrease in absorbance at 315 nm was also accompanied by a concomitant decrease in the original dark purple color of the film-coated substrates that is characteristic of TA-Fe^{III} complexes (by visual inspection; Figure S3 shows a representative example). These observations are generally consistent with past reports on the degradation of hollow TA-Fe^{III} microcapsules upon the addition of EDTA[22] and a recent report describing the erosion of Fe-containing metal-organic frameworks (MOFs) upon the addition of the iron-chelating agent citrate.[48]

Further inspection of Figure 3B reveals that the rates and extents of film erosion were influenced strongly by enterobactin concentration. Film erosion was fastest at concentrations of 8 μM, with >80% of film having eroded within 5 hours. Film erosion also occurred rapidly at 4 μM enterobactin (~80% erosion after 10 hours). In contrast, films eroded much more slowly at concentrations of 2 μM enterobactin—film erosion was only ~25% complete after 24 hours (Figure 3B), and only ~35% complete after 48 hours (Figure S4; transfer of these partially eroded coatings to fresh solutions of 2 μM enterobactin resulted in continued erosion, resulting in ~80% of film loss after 72 hours of incubation). Finally, additional results shown in Figure S5

demonstrate that the erosion of these materials can be arrested by removing them from enterobactin solutions and placing them in fresh buffer, and that further erosion can be triggered by subsequent re-exposure to siderophore. These observed erosion behaviors present the potential to trigger material changes in a siderophore concentration-dependent manner, thus enabling the design of biosensors that respond to bacterial populations *via* secreted siderophores in solution.

The results above demonstrate that the strong Fe^{III} chelator enterobactin can scavenge iron from TA-Fe^{III} based materials and promote disassembly in a concentration-dependent manner. We note that the stability constant of TA-Fe^{III} complexes has been reported to be on the order of 10^9 at pH 5 and 10^{17} at pH 8.[49] These values are substantially smaller than the iron affinity of enterobactin, leading to relatively fast film erosion when these materials are exposed to relatively low concentrations of enterobactin. To determine the impact of siderophore iron affinity on film erosion, we conducted a second set of experiments using the hydroxamate siderophore DFO, which has an iron association constant (10^{30} at neutral pH)[45] that is much lower than enterobactin. Films eroded much more slowly in the presence of DFO and required substantially higher concentrations of siderophore. As shown in Figure S6, film erosion was only 50% complete after 48 hours at concentrations of 200 μM DFO and required ~90 hours to erode completely under these conditions. These differences in erosion profiles are consistent with the large differences in the iron affinities of DFO and enterobactin, and are consistent with the view that the physical erosion observed in these experiments is the result of the extraction of iron by the siderophores.

Disassembly of TA-Fe^{III} Films is Promoted by Enterobactin Produced in Cultures of E. coli

We next performed a series of experiments to determine whether growing cultures of siderophore-producing bacteria could promote the erosion of TA-Fe^{III} coatings. We selected *E. coli* as a model organism for these studies, because the iron uptake and regulation mechanisms of this species are well characterized,[4,50] and we used an iron-poor M9 minimal growth medium that should result in increased production of siderophore.[46] The red curve in Figure 3C shows the erosion profile of TA-Fe^{III} coatings incubated with cultures of wild type (wt) *E. coli* for two days. Inspection of these results shows the films to erode gradually over this time period, with a decrease in absorbance of ~70% after 48 hours. This erosion profile contrasts with that of the M9 medium control (no bacteria), which was relatively stable under these conditions and exhibited a decrease in absorbance of ~10% over the same time period (Figure 3C; blue curve). Characterization of bacterial growth media using Arnow's test, a colorimetric assay used in many past studies to quantify concentrations of catecholate-type siderophores,[33,34] revealed a steady increase in the concentration of siderophore, to ~5 μM after 24 hours and ~10 μM after 48 hours (Figure 3D; red curve). These values are similar to the concentrations of enterobactin used to promote the erosion of otherwise identical coatings in the controlled buffer experiments described above (2-8 μM; Figure 3B).

Taken together, these results are consistent with disruption and disassembly promoted by the secretion of siderophores during bacterial growth. However, these results themselves do not rule out other possibilities, such as other changes to growth medium composition, that could arise during bacterial culture. We therefore conducted a series of additional experiments using two strains of *E. coli* that have been genetically modified to either amplify or disrupt the

production of enterobactin: (i) Δ*entC*, a strain that is unable to synthesize enterobactin under any conditions, and (ii) Δ*fur*, a strain that has been engineered to constitutively overproduce enterobactin. The results of these experiments are shown in Figure 3C, and reveal coatings incubated in cultures of the Δ*entC* mutant strain to exhibit stabilities similar to those of coatings incubated in buffer alone (Figure 3C, light blue curve). In contrast, films incubated in the presence of the Δ*fur* mutant eroded more rapidly than those incubated in the wt *E. coli* control (Figure 3C; green curve). Additional characterization of enterobactin concentrations using Arnow's test revealed these differences in erosion rate to correlate with large differences in the production of enterobactin by these mutant strains (Figure 3D; <1 μM for the Δ*entC* strain and ~30 μM for the Δ*fur* strain after 48 hours of growth).

Overall, the relative rates of erosion observed in Figure 3C for the wt, Δ*entC*, and Δ*fur* strains are consistent with differences in the concentration of enterobactin produced in cultures of these bacteria. Further inspection of the results of experiments using the Δ*entC* mutant reveal a small increase in film erosion relative to the buffer control. We note that while this strain has been engineered to be unable to produce enterobactin, it is still able to biosynthesize small amounts of other, non-catecholate siderophores that could also have the potential to extract iron from these materials.[46] Regardless, we conclude on the basis of these mutant-strain studies that cultures of *E. coli* can trigger the stimuli-responsive disruption and erosion of TA-Fe^{III} coatings through a mechanism that is mediated by the production and secretion of iron-scavenging enterobactin. The results of additional experiments revealed that the large differences in erosion shown in Figure 3C did not arise from changes in environmental pH or differences in the rates of growth of these three bacterial strains (Figures S7-9).

Siderophore-Induced Release of an Antibiotic Agent

We next conducted studies to evaluate the potential of TA-Fe^{III} coatings as a platform for the design of bacteria-responsive materials useful for the siderophore-triggered release of active agents. To explore the feasibility of this approach and demonstrate proof of concept, we focused on the design of TA-Fe^{III} coatings loaded with the broad-spectrum antibiotic ciprofloxacin (CP) for several reasons. First, CP is a potent antimicrobial agent that could serve as a model for the design of new bacteria-responsive coatings that prevent biofouling.[51] Second, CP is a 4-quinolone that has been found to form 3:1 (CP-Fe^{III}) coordination complexes with ferric ions through its pyridine and carboxylate oxygen atoms.[52] Relative to other small-molecule antibiotic agents, we hypothesized that the ability to coordinate to iron could provide a means to anchor CP into the structures of TA-Fe^{III} coatings and minimize or possibly prevent premature diffusion-based burst release prior to film disassembly. Third, CP exhibits fluorescence that can be used to monitor controlled release profiles. While past studies have demonstrated the use of TA-Fe^{III} coatings to coat drug crystals or design hollow capsules or coated particles for the slow or triggered release of loaded agents,[40,42,53,54] we are not aware of past studies in which these materials have been used to trap diffusible, small-molecule active agents within these materials or use them as building blocks and structural elements to design materials for controlled release. We note, however, that structurally ordered Fe-containing MOFs have been widely used to host and release bioactive agents.[48,55-58]

Subsequent experiments demonstrated that CP could be loaded readily into TA-Fe^{III} coatings during film assembly. For these experiments, we used a fabrication protocol similar to the one used in the studies described above, with the exception that TA solutions were substituted with solutions containing mixtures of TA and CP at different molar ratios. Coatings

fabricated using this approach are referred to from here on using the notation $(TA_X:CP_Y\text{-}Fe)_n$, where "X" and "Y" indicate the molar ratios of TA and CP, and "n" denotes the number of deposition cycles. We note, for clarity, that this notation refers only to molar ratios of TA to CP used during assembly and not the amounts of these two agents measured in the films after assembly.

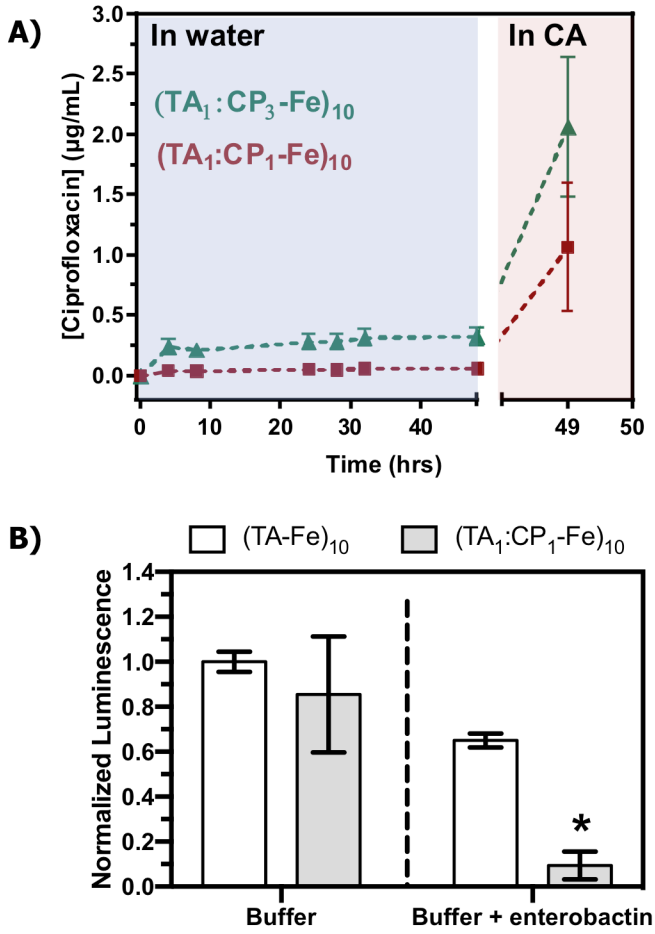

Figure 4. (A) Plot showing the release of ciprofloxacin (CP) from iron-crosslinked TA-Fe^{III} coatings fabricated using two different molar ratios of TA:CP. The data correspond to results using $(TA_1:CP_3\text{-}Fe)_{10}$ films (green triangles) and $(TA_1:CP_1\text{-}Fe)_{10}$ films (red squares) after incubation in 1 mL of water for 48 hours and subsequent incubation for one hour in a solution of citric acid at 37 °C. (B) Plot showing the normalized metabolic activity of *E. coli* strain Δ*entC* after incubation for 24 hours at 37 °C with $(TA\text{-}Fe)_{10}$ or $(TA_1:CP_1\text{-}Fe)_{10}$ coatings in M9 (white bars) and in M9 containing 10 µM enterobactin (grey bars). Results are normalized respect to control consisting of *E. coli* Δ*entC* cultures grown in M9 with $(TA\text{-}Fe)_{10}$ coatings. All results represent the mean ± SEM (n = 3). The asterisk (*) indicates that the differences between the mean value of the result for the $(TA_1:CP_1\text{-}Fe)_{10}$ coatings incubated with 10 µM enterobactin is significantly different compared to all other conditions at a 95% confidence interval ($p < 0.05$) by one-way ANOVA using Tukey's multiple comparison test.

In a first series of experiments, we fabricated coatings having the nominal structure $(TA_1:CP_1\text{-}Fe)_n$, fabricated by solutions containing equimolar amounts of TA and CP. The growth profiles of these coatings, as determined by ellipsometry, were similar to those of TA-Fe^{III} coatings fabricated in the absence of CP (Figure S10), and these films were physically stable and released only very small amounts of CP into solution upon incubation in water for up to two days (as determined by fluorometry; see Figure 4A, red squares). These $(TA_1:CP_1\text{-}Fe)$ films disassembled when exposed to solutions containing enterobactin, however we were unable to accurately measure the amount of CP released into solution under these conditions because the presence of enterobactin resulted in the quenching of ciprofloxacin fluorescence. We therefore conducted a series of similar experiments using solutions of citric acid (an Fe-chelating agent; buffered to pH 2.8) to induce complete erosion of the coating and estimate the amount of CP loaded into the coatings. The addition of citric acid to these materials resulted in triggered erosion and the release of CP into solution (Figure 4A). On the basis of these results, we estimate the total amount of CP loaded into these materials to be 0.29 ± 0.24 μg/cm^2. We note here that incorporation of CP into these materials could occur in at least three ways, including (i) physical entrapment within the network structure, (ii) by hydrogen bonding with TA, or (iii) by coordination to Fe^{III} in competition with TA. While our results do not permit conclusions related to the specific nature of the interactions in the materials used here, the results in Figure 4A indicate that < 5% of the incorporated CP is released prior to the addition of citric acid, and that ~95% is released only after triggered disassembly. We interpret these results to suggest that CP is at least partially bound to film components and cannot readily escape by passive diffusion.

Additional experiments demonstrated that the amount of CP incorporated into these materials could be tuned by adjusting the ratio of TA:CP used during film assembly. Figure 4A

also shows results for the incubation and release of CP from films fabricated using a 1:3 molar ratio of TA:CP (referred to as $(TA_1:CP_3\text{-}Fe)_{10}$ coatings; green triangles). Inspection of these results reveals the total amount of CP loaded into these materials to be 0.61 ± 0.29 μg/cm^2, a two-fold increase over the loading of the $(TA_1:CP_1\text{-}Fe)$ films. Further inspection of these results also reveals, however, a small and rapid burst release during the first four hours of incubation of the $(TA_1:CP_3\text{-}Fe)_{10}$ coatings. This amount of initial release is greater than that observed for $(TA_1:CP_1\text{-}Fe)$ films and corresponds to ~15% of the total CP loaded. Thus, while fabrication at higher molar ratios of CP can be used to increase the overall loading of CP, these loading conditions also lead to more loosely bound CP that can passively diffuse out of the films prior to triggered disassembly. We note that it should also be possible to increase the total amount of CP, or any other incorporated agent, on a surface by increasing the total thickness of the deposited material. Overall, our results indicate that the addition of an iron-chelating agent can be used as a trigger to promote the release of CP contained within these TA-Fe^{III} coatings, and that the amount of loaded agent can be tuned based on fabrication conditions.

CP is a potent broad-spectrum antibiotic active against *E. coli* that is known to inhibit bacterial replication by inhibiting the activity of DNA gyrase and topoisomerase IV enzymes.[51] Building upon the results above, we evaluated the potential of the triggered release of CP from $(TA_1:CP_1\text{-}Fe)_{10}$ coatings to kill *E. coli* cells. Although these $(TA_1:CP_1\text{-}Fe)_{10}$ films contained lower overall loadings of CP than the $(TA_1:CP_3\text{-}Fe)_{10}$ coatings described above, we used them for these experiments because they do not passively release significant amounts of CP prior to siderophore-induced disassembly. Initial experiments using wt *E. coli* conducted by placing film-coated substrates into fresh inoculum did not result in significant cell death after 24 hours (data not shown). We note here that in cultures of wt *E. coli*, enterobactin concentration is generally

low at low population densities and it increases as the cells grow and reach high population densities associated with the stationary phase. The apparent lack of activity in these preliminary experiments thus likely reflected the fact that the release of CP was not triggered immediately at inoculation. Instead, under these experimental conditions, it is likely that CP would be released substantially once the cells were at or near stationary phase (conditions of high population density relative to the amount of CP used here). While it is not surprising that higher concentrations of antibiotic would generally be required to cause cell death once cells have reached the stationary growth phase, past studies have also shown that, for certain strains of *E. coli,* there is a significant decrease in the biocidal efficacy of CP at high population densities,[59] likely related to the mechanism of action of this antibiotic.

In view of the above observations and considerations, we devised a proof-of-concept experiment using cultures of the *E. coli* Δ*entC* mutant strain that is unable to produce enterobactin and supplemented the media with known concentrations of exogenous enterobactin (this strain itself promotes only minimal erosion of TA-Fe^{III} coatings; see Figure 3C). For these experiments, $(TA_1{:}CP_1\text{-}Fe)_{10}$ and control $(TA\text{-}Fe)_{10}$ coatings lacking CP were incubated with cultures of Δ*entC* in the presence or absence of 10 μM enterobactin for 24 hours and the metabolic activity of the cells was characterized using a commercial luciferase assay. Figure 4B shows the results of these experiments normalized to the viability of cells incubated in the presence of control films and buffer only (left side, white bar).

We observed a small but statistically insignificant reduction in cell viability when cultures were incubated in the presence of CP-containing coatings in buffer only (left side, grey bar). However, we observed a large and statistically significant ~90% reduction in cell viability in cultures incubated with CP-containing coatings in the presence of enterobactin (right side,

grey bar) compared to cells grown in the presence of $(TA\text{-}Fe)_{10}$ films alone (and an ~75% reduction in cell viability relative to cells grown in the presence of $(TA_1{:}CP_1\text{-}Fe)_{10}$ coatings without added enterobactin). We also observed a reduction in cell viability in cultures incubated with control $(TA\text{-}Fe)_{10}$ films in the presence of enterobactin (right side, white bars) relative to cultures incubated with control films in the absence of enterobactin (left side, white bar; no significant difference). The reasons for this latter observation are not clear, however we note that the level of viability observed upon triggered disassembly of the CP-containing coatings was ~9 times lower than the levels in those control samples. Overall, these results are consistent with siderophore-induced disassembly and the resulting triggered release of CP at concentrations that are sufficient to substantially kill the populations of cells used in these *in vitro* experiments.

Iron-Crosslinked Alginate Beads Bind to and Sequester Enterobactin

The results above demonstrate that metal/organic networks constructed using iron as a structural building block can be disassembled when exposed to bacterial siderophores that coordinate competitively with and, as a result, extract iron. In that system, the iron extracted by a siderophore can be shuttled into *E. coli* cells and used as a resource, and resultant changes in the composition of the material can lead to large changes in the behaviors of the material. For example, in the studies above, extraction of iron from $TA\text{-}Fe^{III}$ coatings can result in complete disassembly of the materials or be used to promote a stimulus-induced response (*e.g.,* the triggered release of an agent that kills cells). Depending on the structure of a given iron-containing material and the importance of Fe^{III} to its overall stability, structure, or physicochemical properties, we foresee new opportunities to exploit elements of iron homeostasis pathways more broadly to design other types of materials platforms that can respond

to, report on, or interact dynamically with communities of iron-scavenging bacteria. In this section, we report the unexpected discovery of an iron-crosslinked polymer hydrogel that binds to and sequesters enterobactin from surrounding media.

During the course of the studies above, we conducted a series of exploratory experiments to determine whether principles and methods developed for those small-molecule networks could be translated to macromolecular networks crosslinked using Fe^{III}. To evaluate the potential of this approach, we characterized the responses of polymer-based hydrogels, synthesized by the Fe^{III}-induced crosslinking of alginate, to the presence of enterobactin. Alginate is a naturally-derived polysaccharide possessing carboxylate functionality (Figure 1, right) and readily forms hydrogels by ionic crosslinking upon addition of multivalent metal ions.[60] Thus, we hypothesized that the structural and mechanical properties of Fe^{III}-crosslinked alginate gels might be altered by the competitive removal of iron by siderophores. To test this hypothesis, we prepared spherical alginate hydrogel beads ~3 mm in diameter by the extrusion-dripping of a 1% (w/v) alginate solution into a solution of iron sulfate prepared in M9 media (see Materials and Methods section for additional details). After fabrication, these beads were incubated in M9 solutions containing enterobactin at a concentration of 100 μM, a concentration 10 times higher than what is produced by wt *E.coli* cultures after 48 hours of growth (Figure 3D). After one hour of incubation, the appearance of the Fe-alginate beads changed from a characteristic pale orange color to a dark purple color, and after 24 hours of incubation the beads were uniformly dark (Figure 5A).

This dark purple color corresponds to the color previously reported for solutions of enterobactin-Fe^{III} complexes, and suggests the formation of these coordination complexes under these conditions.[61,62] Surprisingly, however, we did not observe the formation of purple color in

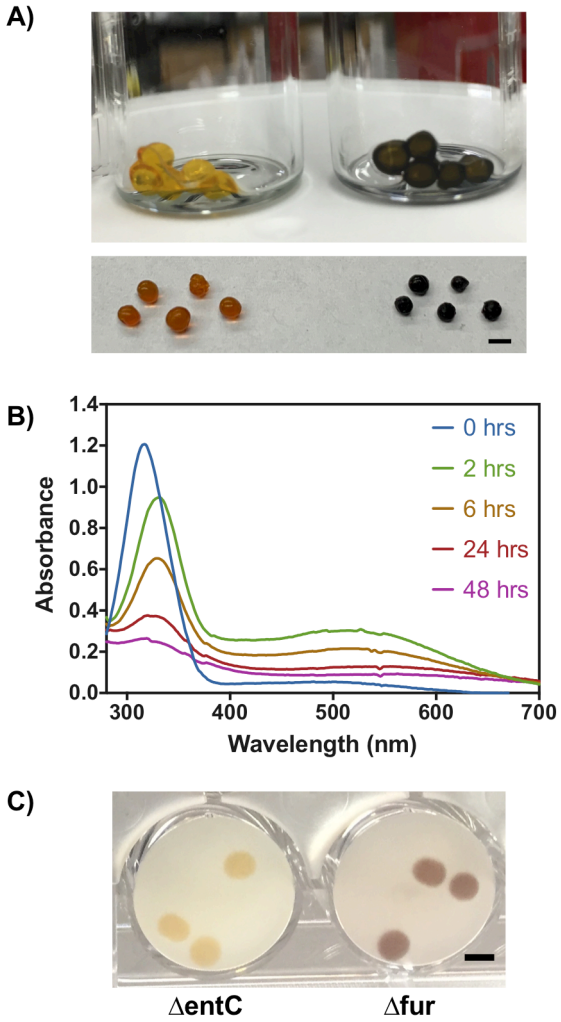

Figure 5. (A) Photographs of Fe-crosslinked alginate beads after incubation for 24 hours in M9 (left; orange color) and in a solution of 100 μM enterobactin in M9 (right; dark purple color). The image in the top photograph shows the beads in vials immediately following preparation/treatment. For clarity, the bottom image shows groups of these beads arranged on a clean white background. (B) UV/vis absorption spectra as a function of time for a solution of enterobactin (100 μM) in M9 incubated with alginate-iron crosslinked beads at 37 °C. (C) Representative photograph of wells of a 24-well plate containing Fe-crosslinked alginate beads incubated with *E. coli* strains Δ*entC* (left) and Δ*fur* (right) for 24 hours at 37 °C in M9 media. Scale bars in (A) and (C) are 3 mm.

solutions surrounding the beads; instead, we observed the color to be confined to the beads themselves. In addition, the beads appeared to be physically stable upon exposure to siderophore; we observed no changes in size or swelling or any other hallmarks of erosion or disassembly of

the beads by visual inspection under these conditions, suggesting that exposure to enterobactin did not substantially alter the density or distribution of crosslinks in the beads. Although this latter observation could potentially stem from the formation of additional crosslinks formed by calcium ions during assembly, as calcium is a component of M9 media and is widely used to form crosslinked alginate hydrogels for other applications, we also observed alginate beads prepared by crosslinking with Fe^{III} in water to be stable under these conditions and exhibit the same behavior. We note, however, that crosslinked alginate beads prepared using Fe^{III} in water, instead of M9, swelled and dissolved when exposed to M9 and were thus insufficiently stable to be used in subsequent experiments. The methods used here resulted in crosslinked alginate beads that were stable in bacterial growth media and at temperatures of 37 °C for at least 72 hours and were suitable for use in all other experiments described below.

When combined, the results above are consistent with the sequestration of enterobactin and/or enterobactin-Fe^{III} complexes on or within these hydrogel beads. To provide additional insight into processes underlying this behavior, we used UV/vis spectrophotometry to characterize changes in the absorbance of solutions of enterobactin incubated in the presence of Fe^{III}-crosslinked alginate beads (at 320 nm, an absorption band characteristic of free enterobactin).[61,62] Inspection of the results in B shows absorbance at 320 nm to decrease steadily over a period of 48 hours, consistent with the removal of enterobactin from solution. Further inspection of these results, however, reveals the appearance of a small absorbance peak at 534 nm, which corresponds to spectra previously reported for enterobactin-Fe^{III} charge-transfer complexes in solution.[61,62] This latter peak is not present in enterobactin solutions (Figure 5B, blue curve), but is present after two hours of incubation with beads (green curve), and then decreases steadily in intensity upon further incubation.

We also observed similar behavior when beads crosslinked in water, rather than M9, were incubated in solutions of enterobactin in water. However, decreases in solution absorbance occurred much more rapidly (~90% reduction in absorbance at 320 nm after only 4 hours of incubation; Figure S11). In addition, we note that the sequestration of iron appeared to be largely irreversible under these conditions. Supernatants incubated with dark purple beads containing sequestered enterobactin-Fe^{III} complexes for 24 hours did not exhibit significant increases in absorption at wavelengths ranging from 320-800 nm (Figure S12). Finally, experiments conducted using alginate beads that were crosslinked with Ga^{III} instead of Fe^{III} did not change color by visual inspection or promote decreases in solution absorbance at 320 nm after 48 hours of incubation with enterobactin in water (Figure S13). We conclude from these experiments that the presence of iron is necessary to promote the sequestration of enterobactin, and that factors associated with the preparation and deployment of these beads (*e.g.,* the composition or ionic strength of the solutions used for crosslinking or to perform sequestration assays) can be used to tune the behaviors of these materials.

The observation of enterobactin-Fe^{III} complexes in solution at early time points in the sequestration experiments above is consistent with at least two possibilities. One possibility is that these complexes could form in solution, facilitated by the initial release of small amounts of Fe^{III} from the beads. Alternatively, these complexes could result from the extraction of Fe^{III} from the beads through a process that involves the penetration of siderophore into the gel and the subsequent diffusion of enterobactin-Fe^{III} complexes back into solution. We consider this latter possibility to be less likely, because (i) the absorption of these enterobactin-Fe^{III} complexes is subsequently observed to decrease, rather than increase, over time and (ii) the purple color associated with the formation of these complexes does not appear to leach from these beads

when they are incubated for prolonged periods in fresh media. We interpret the results above to suggest that any enterobactin-Fe^{III} complexes that do form in solution at early time points are sequestered and removed from solution by the alginate beads. Further support for this possibility is provided by the results of experiments in which solutions containing an equimolar mixture of enterobactin and Fe^{III} were incubated with alginate beads (Figure S14A-B). In those experiments, absorbance at 320 nm was observed to decrease over time (Figure S14B; with associated dynamics of adsorption at 534 nm similar to those discussed above and shown in Figure 5B), the beads were observed to change from pale orange to dark purple in color, and the color of the supernatant solution changed from dark purple to colorless after 72 hours of incubation (Figure S14A).

Our current results do not rule out alternative or other concurrent mechanisms for the sequestration of enterobactin, including mechanisms that may involve the penetration of enterobactin into the gel followed by the formation of enterobactin-Fe^{III} complexes that then remain physically constrained within it. However, we note that the formation of dark purple beads in each of the experiments above is consistent with mechanisms that involve the sequestration of enterobactin-Fe^{III} complexes rather than free enterobactin. Additional studies will be required to understand more completely the factors that govern the interactions of enterobactin and enterobactin-Fe^{III} complexes with these alginate beads. In the context of this current study, however, our results demonstrate materials that can sequester or behave as a "sink" for molecules that bacteria use to scavenge for resources and carry out important biological processes.

Additional support for this view is provided by the results in Figure 5C, which shows alginate beads after incubation with 24-hour inoculums of the Δ*entC* or Δ*fur E. coli* strains.

These images show that beads incubated with the Δ*fur* strain, which continuously expresses enterobactin, turned a dark purple color similar to that observed when beads were incubated with prepared solutions of enterobactin. In contrast, beads incubated with the Δ*entC* strain, which is unable to synthesize enterobactin, retained their original orange color after 24 hours of incubation. We interpret these differences to result from differences in the enterobactin production between these two strains, and conclude that these materials can be used as colorimetric indicators of bacterial enterobactin production. Because these beads are stable in bacterial culture media for prolonged periods, the approaches described here could provide new tools for basic microbiological research. Although not examined as part of this study, the results described here could also provide additional guidance for the design of materials that can interface with, interfere with, or potentially help control the behaviors of communities of iron-scavenging bacteria.

Summary and Conclusions

We have reported the design and characterization of two model Fe-containing soft materials systems that can respond to or interface with bacterial siderophores. Our results demonstrate that metal-organic networks fabricated by crosslinking tannic acid with Fe^{III} disassemble and erode physically when placed in contact with enterobactin or deferoxamine B through a mechanism that involves the extraction of iron. Our results also demonstrate that cultures of wild-type *E. coli*, which naturally produce enterobactin to scavenge iron from their environment, can also trigger the disassembly of these TA-Fe^{III} networks. Additional experiments using mutant strains of *E. coli* revealed erosion by bacterial cultures to occur through a mechanism involving the secretion of enterobactin and not other factors associated

with bacterial growth. This stimuli-responsive behavior was also exploited to design coatings that release the antibiotic CP into bacterial cultures. In a second series of studies, we demonstrated that polymer hydrogels fabricated by the crosslinking of alginate with Fe^{III} do not disassemble in the presence of siderophores, but instead sequester and scavenge enterobactin from surrounding media.

The results reported here provide novel approaches for the design of soft materials that are capable of interfacing with or interfering with biomolecular mechanisms that bacteria use to maintain iron homeostasis, either by yielding useful forms of iron to bacteria or by sequestering iron-scavenging agents from bacteria. Communities of bacteria use siderophores to acquire environmental iron and enable biosynthesis and other life processes, including virulence. Our results thus reveal new bases for the design of soft materials that can respond to or interact dynamically with cultures of iron-scavenging bacteria and, potentially, control their behaviors. The proof-of-concept examples reported here demonstrate materials that respond to siderophores by physically eroding, changing color, or by releasing an active agent. We foresee future opportunities to exploit elements of iron homeostasis pathways to design other types of materials that exhibit other coupled behaviors, thereby enabling new ways to respond to, report on, or influence the behaviors of communities of iron-scavenging bacteria. Polymeric materials that can scavenge siderophores could also provide new tools useful for microbiological research or the development of new clinical treatments to prevent infection.

Acknowledgements. Financial support for this work was provided by the National Science Foundation through a grant provided to the UW–Madison Materials Research Science and Engineering Center (MRSEC; DMR-1720415). The authors acknowledge the use of

instrumentation supported by the NSF through the UW MRSEC (DMR-1720415). B. J. O. was supported in part by the Graduate Research Scholars (GERS) program at UW-Madison and the NIH Chemistry Biology Interface Training Grant (T32 GM008505). We thank Prof. Nicholas L. Abbott for many helpful discussions.

Supporting Information. Additional information on bacterial strains and characterization of materials, including characterization of changes in structure and behavior in contact with siderophores and bacterial cultures (PDF). This material is available free of charge via the Internet at: DOI:

ORCID

Benjamin J. Ortiz: 0000-0001-5016-9427
James Jennings: 0000-0003-1213-4607
David M. Lynn: 0000-0002-3140-8637

References

1. Andrews, S. C.; Robinson, A. K.; Rodríguez-Quiñones, F. Bacterial Iron Homeostasis. *FEMS Microbiol. Rev.* **2003,** *27*, 215-237.

2. Sandy, M.; Butler, A. Microbial Iron Acquisition: Marine and Terrestrial Siderophores. *Chem. Rev.* **2009,** *109*, 4580-4595.

3. Guerinot, M. L. Microbial Iron Transport. *Annu. Rev. Microbiol.* **1994,** *48*, 743-772.

4. Hassan, H.; Troxell, B. Transcriptional Regulation by Ferric Uptake Regulator (Fur) in Pathogenic Bacteria. *Front. Cell. Infect. Microbiol.* **2013,** *3*, 59.

5. McHugh, J. P.; Rodríguez-Quiñones, F.; Abdul-Tehrani, H.; Svistunenko, D. A.; Poole, R. K.; Cooper, C. E.; Andrews, S. C. Global Iron-Dependent Gene Regulation in *Escherichia coli*: A New Mechanism for Iron Homeostasis. *J. Biol. Chem.* **2003,** *278*, 29478-29486.

6. Fong, K. P.; Gao, L.; Demuth, D. R. Luxs and Arcb control Aerobic Growth Of *Actinobacillus actinomycetemcomitans* under Iron Limitation. *Infect. Immun.* **2003,** *71*, 298.

7. Stintzi, A.; Evans, K.; Meyer, J.-m.; Poole, K. Quorum-Sensing and Siderophore Biosynthesis in *Pseudomonas aeruginosa*: Lasrllasi Mutants Exhibit Reduced Pyoverdine Biosynthesis. *FEMS Microbiol. Lett.* **1998,** *166*, 341-345.

8. Lilley, B. N.; Bassler, B. L. Regulation of Quorum Sensing in *Vibrio harveyi* by Luxo and Sigma-54. *Mol. Microbiol.* **2000,** *36*, 940-954.

9. James, C. E.; Hasegawa, Y.; Park, Y.; Yeung, V.; Tribble, G. D.; Kuboniwa, M.; Demuth, D. R.; Lamont, R. J. Luxs Involvement in the Regulation of Genes Coding for Hemin and Iron Acquisition Systems in *Porphyromonas gingivalis*. *Infect. Immun.* **2006,** *74*, 3834.

10. Lewenza, S.; Sokol, P. A. Regulation of Ornibactin Biosynthesis and N-Acyl-L-Homoserine Lactone Production by Cepr in *Burkholderia cepacia*. *J. Bacteriol.* **2001,** *183*, 2212.

11. Post, S. J.; Shapiro, J. A.; Wuest, W. M. Connecting Iron Acquisition and Biofilm Formation in the ESKAPE Pathogens as a Strategy for Combatting Antibiotic Resistance. *MedChemComm* **2019,** *10*, 505-512.

12. Thamphiwatana, S.; Gao, W.; Pornpattananangkul, D.; Zhang, Q.; Fu, V.; Li, J.; Li, J.; Obonyo, M.; Zhang, L. Phospholipase A2-Responsive Antibiotic Delivery via Nanoparticle-Stabilized Liposomes for the Treatment of Bacterial Infection. *J. Mater. Chem. B* **2014,** *2*, 8201-8207.

13. Pornpattananangkul, D.; Zhang, L.; Olson, S.; Aryal, S.; Obonyo, M.; Vecchio, K.; Huang, C.-M.; Zhang, L. Bacterial Toxin-Triggered Drug Release from Gold Nanoparticle-Stabilized Liposomes for the Treatment of Bacterial Infection. *J. Am. Chem. Soc.* **2011,** *133*, 4132-4139.

14. Chen, M.; Xie, S.; Wei, J.; Song, X.; Ding, Z.; Li, X. Antibacterial Micelles with Vancomycin-Mediated Targeting and pH/Lipase-Triggered Release of Antibiotics. *ACS Appl. Mater. Interfaces* **2018,** *10*, 36814-36823.

15. Radovic-Moreno, A. F.; Lu, T. K.; Puscasu, V. A.; Yoon, C. J.; Langer, R.; Farokhzad, O. C. Surface Charge-Switching Polymeric Nanoparticles for Bacterial Cell Wall-Targeted Delivery of Antibiotics. *ACS Nano* **2012,** *6*, 4279-4287.

16. Xiong, M.-H.; Li, Y.-J.; Bao, Y.; Yang, X.-Z.; Hu, B.; Wang, J. Bacteria-Responsive Multifunctional Nanogel for Targeted Antibiotic Delivery. *Adv. Mater.* **2012,** *24*, 6175-6180.

17. Xiong, M.-H.; Bao, Y.; Yang, X.-Z.; Wang, Y.-C.; Sun, B.; Wang, J. Lipase-Sensitive Polymeric Triple-Layered Nanogel for "On-Demand" Drug Delivery. *J. Am. Chem. Soc.* **2012,** *134*, 4355-4362.

18. Ji, H.; Dong, K.; Yan, Z.; Ding, C.; Chen, Z.; Ren, J.; Qu, X. Bacterial Hyaluronidase Self-Triggered Prodrug Release for Chemo-Photothermal Synergistic Treatment of Bacterial Infection. *Small* **2016,** *12*, 6200-6206.

19. Zhuk, I.; Jariwala, F.; Attygalle, A. B.; Wu, Y.; Libera, M. R.; Sukhishvili, S. A. Self-Defensive Layer-by-Layer Films with Bacteria-Triggered Antibiotic Release. *ACS Nano* **2014,** *8*, 7733-7745.

20. Wilson, B. R.; Bogdan, A. R.; Miyazawa, M.; Hashimoto, K.; Tsuji, Y. Siderophores in Iron Metabolism: From Mechanism to Therapy Potential. *Trends Mol. Med.* **2016,** *22*, 1077-1090.

21. Loomis, L. D.; Raymond, K. N. Solution Equilibria of Enterobactin and Metal-Enterobactin Complexes. *Inorganic Chem.* **1991,** *30*, 906-911.

22. Ejima, H.; Richardson, J. J.; Liang, K.; Best, J. P.; van Koeverden, M. P.; Such, G. K.; Cui, J.; Caruso, F. One-Step Assembly of Coordination Complexes for Versatile Film and Particle Engineering. *Science* **2013,** *341*, 154.

23. Zhou, J.; Lin, Z.; Ju, Y.; Rahim, M. A.; Richardson, J. J.; Caruso, F. Polyphenol-Mediated Assembly for Particle Engineering. *Acc. Chem. Res.* **2020,** *53*, 1269–1278.

24. Wang, X.; Jiang, Z.; Shi, J.; Liang, Y.; Zhang, C.; Wu, H. Metal–Organic Coordination-Enabled Layer-by-Layer Self-Assembly to Prepare Hybrid Microcapsules for Efficient Enzyme Immobilization. *ACS Appl. Mater. Interfaces* **2012,** *4*, 3476-3483.

25. Shi, J.; Zhang, L.; Jiang, Z. Facile Construction of Multicompartment Multienzyme System through Layer-by-Layer Self-Assembly and Biomimetic Mineralization. *ACS Appl. Mater. Interfaces* **2011,** *3*, 881-889.

26. Yun, G.; Youn, W.; Lee, H.; Han, S. Y.; Oliveira, M. B.; Cho, H.; Caruso, F.; Mano, J. F.; Choi, I. S. Dynamic Electrophoretic Assembly of Metal–Phenolic Films: Accelerated Formation and Cytocompatible Detachment. *Chem. Mater.* **2020,** *32*, 7746–7753.

27. Carné-Sánchez, A.; Imaz, I.; Cano-Sarabia, M.; Maspoch, D. A Spray-Drying Strategy for Synthesis of Nanoscale Metal–Organic Frameworks and Their Assembly into Hollow Superstructures. *Nat. Chem.* **2013,** *5*, 203-211.

28. Pang, M.; Cairns, A. J.; Liu, Y.; Belmabkhout, Y.; Zeng, H. C.; Eddaoudi, M. Synthesis and Integration of Fe-Soc-Mof Cubes into Colloidosomes via a Single-Step Emulsion-Based Approach. *J. Am. Chem. Soc.* **2013,** *135*, 10234-10237.

29. Chen, J.; Pan, S.; Zhou, J.; Zhong, Q.; Qu, Y.; Richardson, J. J.; Caruso, F. Programmable Permeability of Metal–Phenolic Network Microcapsules. *Chem. Mater.* **2020,** *32*, 6975–6982.

30. Rahim, M. A.; Kempe, K.; Müllner, M.; Ejima, H.; Ju, Y.; van Koeverden, M. P.; Suma, T.; Braunger, J. A.; Leeming, M. G.; Abrahams, B. F.; Caruso, F. Surface-Confined Amorphous Films from Metal-Coordinated Simple Phenolic Ligands. *Chem. Mater.* **2015,** *27*, 5825-5832.

31. Ju, Y.; Cui, J.; Müllner, M.; Suma, T.; Hu, M.; Caruso, F. Engineering Low-Fouling and pH-Degradable Capsules through the Assembly of Metal-Phenolic Networks. *Biomacromolecules* **2015,** *16*, 807-814.

32. Guo, J.; Ping, Y.; Ejima, H.; Alt, K.; Meissner, M.; Richardson, J. J.; Yan, Y.; Peter, K.; von Elverfeldt, D.; Hagemeyer, C. E.; Caruso, F. Engineering Multifunctional Capsules through the Assembly of Metal–Phenolic Networks. *Angew. Chem., Int. Ed.* **2014,** *53*, 5546-5551.

33. Arnow, L. E. Colorimetric Determination of the Components of 3,4-Dihydroxyphenylalanine-Tyrosine Mixtures. *J. Biol. Chem.* **1937,** *118*, 531-537.

34. Winkelmann, G., *Handbook of Microbial Iron Chelates (1991)*. CRC Press: 2017.

35. Rahim, M. A.; Björnmalm, M.; Bertleff-Zieschang, N.; Ju, Y.; Mettu, S.; Leeming, M. G.; Caruso, F. Multiligand Metal–Phenolic Assembly from Green Tea Infusions. *ACS Appl. Mater. Interfaces* **2018,** *10*, 7632-7639.

36. Bertleff-Zieschang, N.; Rahim, M. A.; Ju, Y.; Braunger, J. A.; Suma, T.; Dai, Y.; Pan, S.; Cavalieri, F.; Caruso, F. Biofunctional Metal–Phenolic Films from Dietary Flavonoids. *Chem. Commun.* **2017,** *53*, 1068-1071.

37. Cherepanov, P. V.; Rahim, M. A.; Bertleff-Zieschang, N.; Sayeed, M. A.; O'Mullane, A. P.; Moulton, S. E.; Caruso, F. Electrochemical Behavior and Redox-Dependent Disassembly of Gallic Acid/FeIII Metal–Phenolic Networks. *ACS Appl. Mater. Interfaces* **2018,** *10*, 5828-5834.

38. Liu, P.-Y.; Miao, Z.-H.; Li, K.; Yang, H.; Zhen, L.; Xu, C.-Y. Biocompatible Fe3+–Ta Coordination Complex with High Photothermal Conversion Efficiency for Ablation of Cancer Cells. *Colloids Surf., B* **2018,** *167*, 183-190.

39. Kim, S.; Philippot, S.; Fontanay, S.; Duval, R. E.; Lamouroux, E.; Canilho, N.; Pasc, A. Ph- and Glutathione-Responsive Release of Curcumin from Mesoporous Silica Nanoparticles Coated Using Tannic Acid–Fe(III) Complex. *RSC Adv.* **2015,** *5*, 90550-90558.

40. Shen, G.; Xing, R.; Zhang, N.; Chen, C.; Ma, G.; Yan, X. Interfacial Cohesion and Assembly of Bioadhesive Molecules for Design of Long-Term Stable Hydrophobic Nanodrugs toward Effective Anticancer Therapy. *ACS Nano* **2016,** *10*, 5720-5729.

41. Park, J. H.; Choi, S.; Moon, H. C.; Seo, H.; Kim, J. Y.; Hong, S.-P.; Lee, B. S.; Kang, E.; Lee, J.; Ryu, D. H.; Choi, I. S. Antimicrobial Spray Nanocoating of Supramolecular Fe(III)-Tannic Acid Metal-Organic Coordination Complex: Applications to Shoe Insoles and Fruits. *Sci. Rep.* **2017,** *7*, 6980.

42. Huang, H.; Li, P.; Liu, C.; Ma, H.; Huang, H.; Lin, Y.; Wang, C.; Yang, Y. pH-Responsive Nanodrug Encapsulated by Tannic Acid Complex for Controlled Drug Delivery. *RSC Adv.* **2017,** *7*, 2829-2835.

43. Zhong, Q.-Z.; Pan, S.; Rahim, M. A.; Yun, G.; Li, J.; Ju, Y.; Lin, Z.; Han, Y.; Ma, Y.; Richardson, J. J.; Caruso, F. Spray Assembly of Metal–Phenolic Networks: Formation, Growth, and Applications. *ACS Appl. Mater. Interfaces* **2018,** *10*, 33721-33729.

44. Schupp, T.; Toupet, C.; Divers, M. Cloning and Expression of Two Genes of Streptomyces Pilosus Involved in the Biosynthesis of the Siderophore Desferrioxamine B. *Gene* **1988,** *64*, 179-188.

45. Anderegg, G. v.; l'Eplattenier, F.; Schwarzenbach, G. Hydroxamatkomplexe II. Die Anwendung Der pH‐Methode. *Helv. Chim. Acta* **1963,** *46*, 1400-1408.

46. Valdebenito, M.; Crumbliss, A. L.; Winkelmann, G.; Hantke, K. Environmental Factors Influence the Production of Enterobactin, Salmochelin, Aerobactin, and Yersiniabactin in *Escherichia coli* Strain Nissle 1917. *Int. J. Med. Microbiol.* **2006,** *296*, 513-520.

47. Shutava, T.; Prouty, M.; Kommireddy, D.; Lvov, Y. pH Responsive Decomposable Layer-by-Layer Nanofilms and Capsules on the Basis of Tannic Acid. *Macromolecules* **2005,** *38*, 2850-2858.

48. Claes, B.; Boudewijns, T.; Muchez, L.; Hooyberghs, G.; Van der Eycken, E. V.; Vanderleyden, J.; Steenackers, H. P.; De Vos, D. E. Smart Metal–Organic Framework Coatings: Triggered Antibiofilm Compound Release. *ACS Appl. Mater. Interfaces* **2017,** *9*, 4440-4449.

49. Sungur, Ş.; Uzar, A. Investigation of Complexes Tannic Acid and Myricetin with Fe(III). *Spectrochim. Acta, Part A* **2008,** *69*, 225-229.

50. McHugh, J. P.; Rodríguez-Quiñones, F.; Abdul-Tehrani, H.; Svistunenko, D. A.; Poole, R. K.; Cooper, C. E.; Andrews, S. C. Global Iron-Dependent Gene Regulation in *Escherichia coli*: A New Mechanism for Iron Homeostasis. *Journal of Biological Chemistry* **2003,** *278*, 29478-29486.

51. Drlica, K.; Zhao, X. DNA Gyrase, Topoisomerase IV, and the 4-Quinolones. *Microbiol. Mol. Biol. Rev.* **1997,** *61*, 377.

52. Badal, S.; Her, Y. F.; Maher, L. J. Nonantibiotic Effects of Fluoroquinolones in Mammalian Cells. *J. Biol. Chem.* **2015,** *290*, 22287-22297.

53. Chen, Y.; Wang, J.; Liu, J.; Lu, L. Metal-Phenolic Encapsulated Mesoporous Silica Nanoparticles for pH-Responsive Drug Delivery and Magnetic Resonance Imaging. *Zeitschrift für Physikalische Chemie* **2018,** *232*, 1733-1740.

54. Guo, J.; Suma, T.; Richardson, J. J.; Ejima, H. Modular Assembly of Biomaterials Using Polyphenols as Building Blocks. *ACS Biomater. Sci. Eng.* **2019,** *5*, 5578-5596.

55. Wang, X.; Li, X.; Liang, X.; Liang, J.; Zhang, C.; Yang, J.; Wang, C.; Kong, D.; Sun, H. Ros-Responsive Capsules Engineered from Green Tea Polyphenol–Metal Networks for Anticancer Drug Delivery. *J. Mater. Chem. B* **2018,** *6*, 1000-1010.

56. An, J.; Geib, S. J.; Rosi, N. L. Cation-Triggered Drug Release from a Porous Zinc−Adeninate Metal−Organic Framework. *J. Am. Chem. Soc.* **2009,** *131*, 8376-8377.

57. Miller, S. R.; Heurtaux, D.; Baati, T.; Horcajada, P.; Grenèche, J.-M.; Serre, C. Biodegradable Therapeutic MOFs for the Delivery of Bioactive Molecules. *Chem. Commun.* **2010,** *46*, 4526-4528.

58. Rojas, S.; Colinet, I.; Cunha, D.; Hidalgo, T.; Salles, F.; Serre, C.; Guillou, N.; Horcajada, P. Toward Understanding Drug Incorporation and Delivery from Biocompatible Metal–Organic Frameworks in View of Cutaneous Administration. *ACS Omega* **2018,** *3*, 2994-3003.

59. Zeiler, H. J. Evaluation of the in vitro Bactericidal Action of Ciprofloxacin on Cells of *Escherichia coli* in the Logarithmic and Stationary Phases of Growth. *Antimicrob. Agents Chemother.* **1985,** *28*, 524-527.

60. Agulhon, P.; Robitzer, M.; Habas, J.-P.; Quignard, F. Influence of Both Cation and Alginate Nature on the Rheological Behavior of Transition Metal Alginate Gels. *Carbohydr. Polym.* **2014,** *112*, 525-531.

61. Salama, S.; Stong, J. D.; Neilands, J. B.; Spiro, T. G. Electronic and Resonance Raman Spectra of Iron (III) Complexes of Enterobactin, Catechol, and N-Methyl-2,3-Dihydroxybenzamide. *Biochemistry* **1978,** *17*, 3781-3785.

62. Banerjee, S.; Weerasinghe, A. J.; Parker Siburt, C. J.; Kreulen, R. T.; Armstrong, S. K.; Brickman, T. J.; Lambert, L. A.; Crumbliss, A. L. Bordetella Pertussis Fbpa Binds Both Unchelated Iron and Iron Siderophore Complexes. *Biochemistry* **2014,** *53*, 3952-3960.

For Table of Contents Use Only: